Laser and Particle Beams (2016), *34*, 61–71.

doi:10.1017/S0263034615000919

Diagnosing dense and magnetized plasmas irradiated by a petawatt laser

C. DEUTSCH,[1] H.B. NERSISYAN,[2] AND A. BENDIB[3]

[1]LPGP, CNRS, Univ. Paris-Sud, Université Paris-Saclay, Orsay, France
[2]Radiophysics Institute-Yerevan, Armenia
[3]Quantum Electronic Laboratory, Faculty of Sciences, USTHB, Algiers, Algeria

(Received 20 February 2015; Accepted 18 May 2015)

Abstract

We survey the present status and potentialities of diagnostics for arbitrary magnetized plasmas of inertial confinement fusion concern. These diagnostics include: Faraday rotation, inverse Faraday effect, Thomson scattering, Stark–Zeeman line broadening as well as proton stopping for any ratio, of the particles plasma frequency to cyclotron frequency. This presentation is timely motivated by recent experiments highlighting laser-produced kilo Teslas and nearly steady magnetic fields in inertial fusion plasmas. Positive synergies due to diagnostics combinations are also addressed.

Keywords: Dense and magnetized plasmas; Diagnostic; Low velocity ion slowing down

1. INTRODUCTION

1.1. General

For the last few years, or so, a sudden and strong interest for strongly magnetized plasmas has emerged on an international scale within the inertial confinement fusion (ICF) dedicated community. Certainly, it is related to the very stringent conditions demanded by a successful laser driven implosion of the thermonuclear pellet, as evidenced by the last national ignition facility (NIF) campaign at Lawrence Livermore National Laboratory (LLNL) – Livermore.

Simultaneously, very encouraging demonstration of a nearly steady, on a ns-time scale, kilo-Tesla magnetic field resulting from a laser irradiated coil (Fujioka *et al.*, 2013) has prompted the perspective of using strong applied magnetic (B) intensities to control the laser–plasma interaction, itself.

In this context, it appears highly timely to survey the diagnostics of magnetized plasmas. We try to fulfill this goal by focusing attention on:

- Faraday rotation
- Inverse Faraday effect (IFE)
- Thomson scattering (TS)
- Combined Stark–Zeeman line broadening of hydrogenic transitions (dipolar)
- Proton and heavier ion stopping in dense and arbitrary magnetized plasmas and as a prerequisite, we first survey the commonly used parameters in a no field situation ($B = 0$) and a magnetized one ($B \neq 0$) (Potekhin & Chabrier, 2012).

1.2. General parameters

The state of a free-electron gas is determined by the electron number density n_e and temperature T. Instead of n_e it is convenient to introduce the dimensionless density parameter $r_s = a_e/a_0$, where a_0 is the Bohr radius and $a_e = (4/3\pi n_e)^{-1/3}$. The parameter r_s can be quickly evaluated from the relations $r_s = 1.1723 n_{24}^{-1/3} = (\rho_0/\rho)^{1/3}$, where $n_{24} \equiv n_e/10^{24}$ cm^{-3} and $\rho_0 = 2.6752(A/Z)$g/cm^3. The analogous density parameter for the ions is $R_S = a_i m_i (Ze)^2/\hbar^2 = 1822.89 A Z^{7/3} r_s$, where m_i is the ion mass and $a_i \equiv (4/3\pi n_i)^{-1/3}$ is the ion sphere radius while electron degeneracy is $\theta = T/T_F$. In the nonrelativistic limit, $T_F \approx 1.163 \times 10^6 r_s^{-2}$ K, and

$$\theta = 0.543\, r_s/\Gamma_e,$$

where

$$\Gamma_e \equiv \frac{e^2}{a_e k_B T} \approx \frac{22.747}{T_6}\left(\rho_6 \frac{Z}{A}\right)^{1/3}$$

Address correspondence and reprint requests to: C. Deutsch, LPGP-U-Paris-Sud, (UMR-CNRS 8578), Orsay, France. E-mail: claude.deutsch@u-psud.fr

The strength of the Coulomb interaction of nonrelativistic ions is characterized by the Coulomb coupling parameter

$$\Gamma = \frac{(Ze)^2}{a_i k_B T} = \Gamma_e Z^{5/3},$$

where $T_6 \equiv T/10^6$ K.

1.3. Magnetic parameters

Convenient dimensionless parameters that characterize the magnetic field in a plasma are the ratios of the electron cyclotron energy $\hbar\omega_c$ to the Hartree unit of energy, to the electron rest energy, and to $k_B T$:

$$\gamma_m = \hbar^3 B/m_e^2 c e^3 = B/B_0,$$

where $B_0 = 2.3505 \times 10^9 G$,

$$b = \frac{\hbar\,\omega_c}{m_e c^2} = \alpha_f^2 \gamma_m = \frac{B}{4.414 \times 10^{13} G},$$

where $\alpha_f = e^2/\hbar c$ is the fine-structure constant, and

$$\zeta = \hbar\omega_c/k_B T \approx 134.34 B_{12}/T_6$$

where $B_{12} \equiv B/10^{12} G$. The magnetic length $a_m = (\hbar c/eB)^{1/2} = a_0/\sqrt{\gamma_m}$ gives a characteristic transverse scale of the electron wave function.

For the ions, the cyclotron energy is $\hbar\omega_{ci} = Z(m_e/m_i)\hbar\omega_c$, and the parameter analogous of ζ is

$$\zeta_i = \hbar\omega_{ci}/k_B T \approx 0.0737(Z/A)B_{12}/T_6.$$

Another important parameter is the ratio of the ion cyclotron frequency to the plasma frequency,

$$\beta = \omega_{ci}/\omega_p = \zeta_i/\eta \approx 0.0094 B_{12}\sqrt{\rho_6}.$$

2. FARADAY ROTATION

In 1845 Michael Faraday discovered that a longitudinal magnetic field can rotate the polarization direction of light passing through transparent dielectric material. That discovery was, in fact, the first empirical connection between light and magnetism.

In interstellar space, Faraday rotation is most easily seen in linearly polarized radio beams traversing a region of magnetized plasma. The resulting rotation $\Delta\theta$ of the beam's polarization direction is given by $\Re\lambda^2$, where λ is the radio wavelength and $\Re$, the so-called rotation measure, is an integral over the observer's line of sight to the radio source.

In Gaussian units, it is given by

$$\Re = (e^3/2\pi m^2 c^4) \int n_e(s) B_s(s) ds, \quad (1)$$

where n_e is the local density of free electrons, m is the electron mass, and B_s is the local magnetic field's component along the line of sight.

3. THE IFE

The IFE is the phenomenon where a magnetic field is created in a medium due to the rotation of the electric field (Eliezer, 2002). In particular, a circularly polarized laser can induce a magnetic field in the plasma. The magnetic field arises because the electrons quiver with the oscillating electric field of the incoming laser light, and if the laser is circularly polarized then the electrons describe a circular motion. The net effect of this is a circular current on the edge of the plasma, which generates the magnetic field (see Fig. 1).

A simple (order of magnitude) calculation for the magnetic field created by the IFE in cold plasma is now developed. The motion of the electrons in an applied electric field is, according to linearized law,

$$\frac{\partial v}{\partial t} = -\frac{e}{m_e}\mathbf{E} \quad (2)$$

where $\mathbf{v}$ is the electron velocity and $\mathbf{E}$ is the applied electric field in the plasma, as a result of the absorbed laser energy. The ions are considered immobile. The electric field is incident in the z-direction and is circularly polarized in the x–y plane:

$$\mathbf{E} = E_0\left(\frac{\hat{\mathbf{x}} + \mathbf{i}\hat{\mathbf{y}}}{\sqrt{2}}\right)\exp[-i(\omega t - kz)] \quad (3)$$

where $\hat{\mathbf{x}}$ and $\hat{\mathbf{y}}$ are unit vectors in the x- and y-directions, respectively.

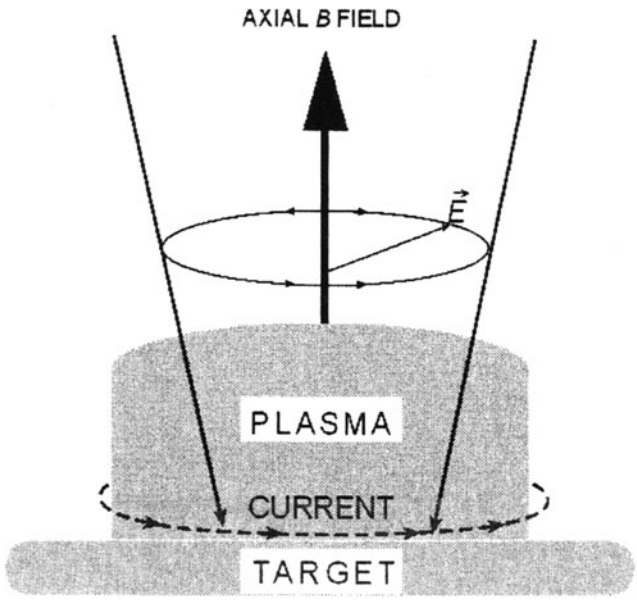

Fig. 1. A schematic presentation of the inverse Faraday effect (after (Eliezer, 2002)).

https://doi.org/10.1017/S0263034615000919 Published online by Cambridge University Press

Substituting (3) into (2), one gets the solution for the electron (fluid) velocity:

$$\mathbf{v} = v_0\left(\frac{-\hat{\mathbf{x}} + \mathbf{i}\hat{\mathbf{y}}}{\sqrt{2}}\right)\exp[-i(\omega t - kz)], \quad v_0 = \frac{eE_0}{m_e\omega} \tag{4}$$

The electrons also satisfy the continuity equation

$$\frac{\partial n_e}{\partial t} = -\nabla\cdot(n_e\mathbf{v}). \tag{5}$$

The density is assumed to consist of a background (n_0) and perturbed (n_1) components

$$n_e = n_0 + n_1 \qquad n_0 \gg n_1 \tag{6}$$

where n_0 does not depend on time and $n_1 \approx \exp(-i\omega t)$. Since $\nabla\cdot\mathbf{v} = 0$, the continuity Eq. (5) yields

$$i\omega n_1 = \mathbf{v}\cdot(\nabla n_0). \tag{7}$$

The electric current, which in this approximation is a second-order perturbed value, is obtained by using (4) and (7):

$$\mathbf{J} = -e\langle n_1\mathbf{v}\rangle = \left\langle\frac{ie}{\omega}(\mathbf{v}\cdot\nabla n_0)\mathbf{v}\right\rangle = \frac{e^3E_0^2}{2m_e\omega^3}\nabla n_0\times\hat{\mathbf{z}} \tag{8}$$

where $\langle\rangle$ is the time average over the fast oscillations and $\hat{\mathbf{z}}$ is the unit vector in the z-direction. Note that the wave vector of the electromagnetic field is parallel to $\hat{\mathbf{z}}$. From Eq. (8) one can see that the electric current $\mathbf{J}$ has a contribution from the density gradient in the x–y plane (mainly from the edge of the plasma) and it points in the toroidal direction. This current produces an axial magnetic field (i.e., in the z-direction) according to Maxwell's equation (Gaussian units):

$$\nabla\times\mathbf{B} = \frac{4\pi}{c}\mathbf{J},$$

which in order of magnitude is given by

$$B = \frac{\omega_p^2}{\omega^3}\frac{e}{mc}|E|^2 \tag{9}$$

where ω_p is the electron plasma frequency. This may be expressed in terms of the laser light intensity I_L by

$$I_L = \frac{c}{4\pi}|E|^2.$$

Thus, we find the axial poloidal magnetic field

$$\frac{B}{gauss} = 2\times10^{-10}\frac{I_L}{W/\mathrm{cm}^2}\left(\frac{\lambda}{1\,\mu\mathrm{m}}\right)^3\left(\frac{n}{10^{21}\,\mathrm{cm}^{-3}}\right). \tag{10}$$

where λ is the laser wavelength. For instance, taking $\lambda = 1\,\mu$m, as for a neodymium laser, and $n = 10^{21}\,\mathrm{cm}^{-3}$, with $I_L = 10^{16}W/\mathrm{cm}^2$, gives $B = 2\times10^6$ Gauss. As a second example, suppose $\lambda = 10\,\mu$m, as in a CO_2 laser, $n = 10^{19}\mathrm{cm}^{-3}$, and $I_L = 10^{14}W/\mathrm{cm}^2$. We kept $I_L\lambda^2$ constant in the two examples, as this seems to be the case in practice. For this example, $B = 2\times10^5$ gauss.

This derivation highlights a classical dipole approximation.

Using ponderomotive forces (Lehner, 1994), it was suggested that the induced magnetic field is not linear with I_L, as given by the classical IFE (10), but B is proportional to the square root of I_L. Moreover, the constant of proportionality is significantly larger than in the classical approach. In this formalism the electric current is a first-order effect rather than a second-order perturbation value. In the non-relativistic domain the axial magnetic field, can thus be written as

$$B = B_c\left(\frac{\omega_{pe}}{\omega}\right)\left(\frac{eE_0}{m_e\omega c}\right) \approx 6.5\times10^5\left(\frac{n_e}{n_e c}\right)^{1/2}\left(\frac{I_L}{10^{14}\,\mathrm{Watt/cm}^2}\right)^{1/2}. \tag{11}$$

This formula fits some experiments (Horovitz *et al.*, 1997) in the domain of $I_L \approx 10^{10}\,W/\mathrm{cm}^2$. However, for $\sim10^{14}$ Watt/cm^2 the experimental values are larger than those estimated by Eq. (11).

It has also been stressed (Talin *et al.*, 1975) that the IFE strongly relies on angular momentum transfer between radiation field and plasma as evidenced by a Kubo response function formalism. Up to now, experiments have not yet been discriminated amongst the above theory proposals.

Apparently, the very first manifestations of IFE in plasmas have been identified with a Klystron source of waves (Deschamps *et al.*, 1970).

Currently, high power lasers are used.

Magnetic fields in excess of 7 MG have been measured with high spatial and temporal precision during interactions of a circularly polarized laser pulse with an underdense helium plasma at intensities up to 10^{19} Watt/cm^2 (Najmudin *et al.*, 2001). The fields, while of the form expected from the IFE for a cold plasma, are much larger than expected, and have a duration approaching that of the high intensity laser pulse (<3 psec). These observations can be explained by particle-in-cell (PIC) simulations in 3D. The simulations show that the magnetic field is generated by fast electrons which spiral around the axis of the channel created by the laser field.

More generally, 3D PIC simulations allow for a detailed analysis of a given experiment, while deeper theoretical investigations are still lacking in this area of magnetized plasmas.

4. PLASMA SCATTERING OF ELECTROMAGNETIC RADIATION: TS

4.1. General

It is well-known that electromagnetic radiation is emitted by an accelerated charge. An important example of this

https://doi.org/10.1017/S0263034615000919 Published online by Cambridge University Press

phenomenon occurs when the acceleration is induced in the first place by an electromagnetic wave. This interaction, when the incident radiation is of sufficiently low frequency ω so that $\hbar\omega$ is much less than mc^2, the rest energy of the charge, is generally referred to as TS.[1] It is the extension of the theory to include the simultaneous scattering from a large number of free positive and negative charges, that is, the plasma, and the experimental application of scattering, which are the topics of concern.

For a single charge the angular distribution of intensity, the frequency, and the phase of the scattered radiation depend on the orbit of that charge relative to the observer. Equally, for a large group of charges the scattered spectrum is related to the orbits of all those charges, or rather in practice, to some average taken over the probable behavior of the group. From the spectrum of radiation scattered from a plasma we may in principle determine the electron and ion temperatures and densities, the direction and magnitude of a magnetic field in the plasma, and in general, information about all fluctuations (waves, instabilities) within the plasma. In reality, we are of course limited by the radiation sources available to us; the cross-section for scattering is so small that measurements on laboratory plasmas were not possible at all until the advent of high-power lasers. The first measurements were by the scattering of radio waves from the ionosphere in the late 1950s.

4.2. Stokes parameters for TS in magnetized plasma

We consider the scattering of a plane monochromatic electromagnetic wave by an electron located at the origin of a Cartesian coordinate system, in a cold collisionless plasma in a uniform magnetic field. Let **B** be a uniform static magnetic field pointing in the direction of the z-axis, $\mathbf{B} = B\hat{\mathbf{z}}$, where $\hat{\mathbf{z}}$ represents the unit vector and B denotes the field strength (Chou & Chen, 1994).

The propagation vector **k** of the incident electromagnetic wave makes an angle α with the static magnetic field, and is lying in the xz-plane as shown in Figure 2.

To calculate the polarization parameters due to magnetic TS we first resolve the $\mathbf{E}(t)$ vector of the incident wave into parallel ($E_\parallel(t)$) and perpendicular ($E_\perp(t)$) components with respect to the xz-plane formed by the static external magnetic field **B** and the direction of propagation of the incident wave. The intensity of the incident wave may therefore be written in terms of these two transverse components and the longitudinal component E_L in the direction of propagation

$$\mathbf{E}^* \cdot \mathbf{E} = E_\parallel^* E_\parallel + E_\perp^* E_\perp + E_\mathrm{L}^* E_\mathrm{L}\,, \tag{12}$$

as shown in Figure 2,

[1]TS is a limiting case of *Compton* scattering applicable at low enough frequencies so that the photon energy is much less than the charge rest energy, so that quantum effects may be neglected.

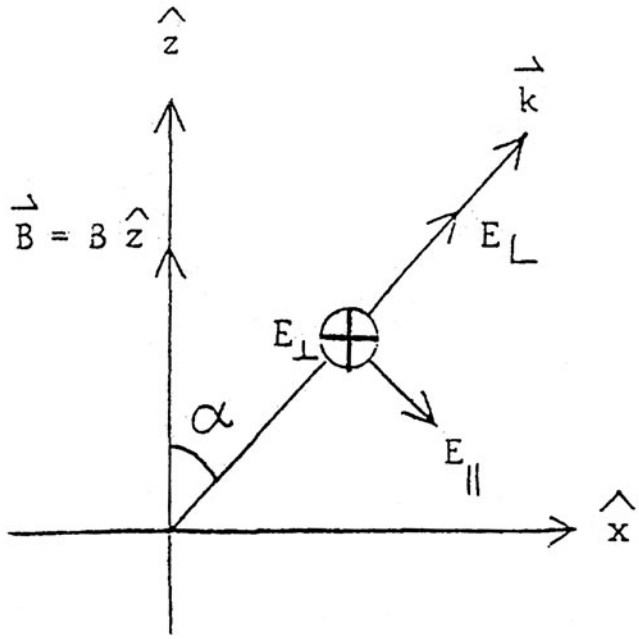

Fig. 2. Thomson scattering in a magnetized plasma. $E_\parallel$ is in xz-plane, $E_\perp$ is perpendicular to xz-plane, E_L is along the propagation vector **k**, $\alpha < (\mathbf{k}, \mathbf{B})$, **B** denotes a static uniform magnetic field.

The Stokes parameters which describe the intensity and polarization of the incident electromagnetic wave propagating in a magnetized plasma will now be written in terms of the parallel and perpendicular electric field components $E_\parallel$ and $E_\perp$ as

$$\begin{aligned} I &\equiv S_0 = E_\parallel^* E_\parallel + E_\perp^* E_\perp, \\ Q &\equiv S_1 = E_\parallel^* E_\parallel - E_\perp^* E_\perp, \\ U &\equiv S_2 = E_\parallel^* E_\perp + E_\perp^* E_\parallel \\ V &\equiv S_3 = -i(E_\parallel^* E_\perp + E_\perp^* E_\parallel). \end{aligned} \tag{13}$$

We note that for electromagnetic waves propagating in a plasma, there is generally, also an electric field in the direction of propagation, namely, the longitudinal component $E_\mathrm{L} = E_\mathrm{L}\hat{\mathbf{k}}$ where $\hat{\mathbf{k}}$ is a unit vector in the direction of propagation.

The first Stokes parameter I simply gives the intensity of the radiation, the second Q and third U specify the linear polarization, and the fourth V, the circular polarization. The effect of the magnetized plasma on the scattered radiation may then be determined by the following set of Stokes parameters in a symbolic matrix form

$$\vec{M}' = \frac{r_0^2}{R^2}\vec{M}\cdot\vec{S},$$

where

$$\begin{aligned} \vec{S} &= (I, Q, U, V) = (S_0, S_1, S_2, S_3), \\ \vec{S}' &= (I', Q', U', V') = (S'_0, S'_1, S'_2, S'_3) \end{aligned} \tag{14}$$

https://doi.org/10.1017/S0263034615000919 Published online by Cambridge University Press

are the 4-vectors constructed with the Stokes parameters for the incident and scattered radiation, with

$$r_0 = e^2/mc^2 = 2.83 \times 10^{-13}\ \text{cm}$$

$\hat{\mathbf{r}} = \mathbf{R}/R$ a unit vector directed from the position of the charge to the observation point, and R is the distance between the two points.

If the incident wave is linearly polarized with its electric field perpendicular to the external magnetic field, the scattered wave is in general elliptically polarized. The polarization of the scattered wave becomes linear only if the observation is made in the plane perpendicular to the magnetic field in view of azimuthal symmetry of the scattering relative to the static magnetic field. The Stokes parameters of the scattered radiation are significantly reduced in the regime of low frequency and strong magnetic field ($\Omega_c \ll \omega \ll \omega_c$) due to the presence of the magnetized plasma. Plasma effects are relatively small and insensitive to the value of $\vee$ ($\vee \equiv \omega_p^2/\omega^2$) as long as $\vee \ll 1$.

For TS in a cold magnetized plasma, the total cross-section may thus be cast in the form ($u = \omega_c^2/\omega^2$)

$$\sigma_\lambda(\omega, B) = \frac{\sigma_T}{[1 + K_\lambda^2(\alpha) + L_\lambda^2(\alpha)]} \times \Big\{[k_\lambda(\alpha)\sin\alpha + L_\lambda(\alpha)\cos\alpha]^2 + \frac{1}{(1-u)^2}[1 - u^{1/2}(K_\lambda(\alpha)\cos\alpha - L_\lambda(\alpha)\sin\alpha]^2 + \frac{1}{(1-u)^2}[u^{1/2} - K_\lambda(\alpha)\cos\alpha - L_\lambda(\alpha)\sin\alpha]^2\Big\}, \tag{15}$$

where α is the angle of incidence relative to the static magnetic field $\mathbf{B}$ and $\sigma_T = 8\pi r_0^2/3$ denotes the canonical Thomson cross-section, where

$$K_\lambda(\alpha) = \frac{2u^{1/2}(1-\vee)\cos\alpha}{u\sin^2\alpha - (-1)^\lambda\sqrt{u^2\sin^4\alpha + 4u(1-\vee)^2\cos^2\alpha}},$$

and

$$L_\lambda(\alpha) = \frac{2u^{1/2}\vee\sin\alpha}{2(1-\vee) - u\sin^2\alpha + (-1)^\lambda\sqrt{u^2\sin^4\alpha + 4u(1-\vee)^2\cos^2\alpha}}$$

with $\lambda = 1$ mode designating the extraordinary wave and $\lambda = 2$ mode the ordinary wave.

The r_0^2-scaling of $\sigma_\lambda(\omega, B)$ thus highlights a m^{-2} dependence featuring an overwhelming electron contribution to TS, while the e^4-dependence demonstrates that only very highly charged ion could substantially contribute to TS. We have in this way documented incoherent scattering by independent electrons.

Correlated (Coherent) redistribution of incoming radiation should be expected in a hot plasma. Up to now, that situation has only been taken up in the highly dilute magnetized plasmas encountered in Tokamak-like machines, (Sheffield, 1975). TS in dense and magnetized plasmas of ICF concern seems to be still awaiting for a dedicated treatment. A very recent experimental demonstration of TS in a magnetized plasma had just appeared (Kenmochi *et al.*, 2014).

5. STARK–ZEEMAN BROADENING OF HYDROGENIC TRANSITIONS

The standard impact formalism (Griem, 1964; Bekefi *el al.*, 1976) for line broadening by plasma may be easily extended to take into account the full es-structure of the static patterns in presence of combined Stark and Zeeman effects.

Then the light intensity polarized along a unit vector $\hat{\mathbf{e}}$ may be written

$$I(\omega, \hat{\mathbf{e}}) = \pi^{-1}\text{Re}\int W(\vec{F})d\vec{F}\sum_{i,j,k,l}\langle n_i|\hat{\mathbf{e}}\cdot\vec{R}|n_j\rangle \times\langle n'k|\hat{\mathbf{e}}\cdot\vec{R}|nl\rangle\langle n_i|\langle n_j|\{i[\omega - \hbar^{-1}(H_n - H_{n'})] - \phi_{nn'}\}^{-1}|nl\rangle|n'k\rangle, \tag{16}$$

with $\vec{R}$ the optical electron position vector. $H_n[H_{n'}]$ is the atomic Hamiltonian taking into account the full static electromagnetic perturbation operating on the sublevels $|n_i\rangle$ and $|n_l\rangle$ of the upper state $(n)[|n_j\rangle$ and $|n_k\rangle$ of the lower state $(n')]$ of the line. $\phi_{nn'}$ denotes the electron collision (or relaxation) operator.

As in most line-broadening theories, the ions are regarded as infinitely massive classical particles over the time of interest (static ion approximation). Moreover, it may be shown that the low-frequency microfield distribution $W(\vec{F})$ is rigorously unaffected in presence of a magnetic field of any strength when Doppler broadening is negligible in a thermal plasma. Therefore, it remains to evaluate the $\phi_{nn'}$ matrix elements. We restrict our attention to a sufficiently high electron density, such that the Larmor radius remains greater than the corresponding Debye length, that is,

$$r_G/\lambda_D = 4.544 \times 10^{-3} N_e^{1/2}/H \geq 1, \tag{17}$$

where N_e is in cm^{-3} and H in gauss.

The electron–atom interaction may then be evaluated with the usual monopole–dipole approximation and a straight-line trajectory for the perturbing electron traveling in the Debye sphere surrounding the emitter.

Relative strength of Stark to Zeeman line shift features

$$\tau = \frac{3}{2}n(n-1)ea_0E_0/\frac{(n-1)e\hbar H}{2mc} = \frac{3}{2}nA_0 \qquad A_0 = 3.43 \times 10^{-7} N_e^{2/3}[\text{cm}^{-3}]/H \tag{18}$$

for the $\mathcal{H}$-atom like emitter.

https://doi.org/10.1017/S0263034615000919 Published online by Cambridge University Press

Pure Stark broadening is retrieved with $\tau \gg 1$ (large n and N_e moderate H. Line profiles depend on the direction of observation. The magnetic field $\vec{H}$ polarizes the emitted light.

Averaging the usual impact profiles around the direction of the magnetic field, yields the complete profiles including averages on the plasma microfield, which are polarized either along or transverse to the magnetic field. This procedure is illustrated in Figures 3 and 4, (Nguyen - Hoe *et al.*, 1967) for the H_α lines of atomic hydrogen observed either parallel or perpendicular to $\vec{H}$ and expressed in terms of the polarized intensities by the relations

$$I_{\parallel}(\Delta\lambda) = \frac{1}{2}[I(\Delta\lambda, \hat{\mathbf{x}}) + I(\Delta\lambda, \hat{\mathbf{y}})]$$
$$I_{\perp}(\Delta\lambda) = \frac{1}{2}[I_{\parallel}(\Delta\lambda, \hat{\mathbf{x}}) + I(\Delta\lambda, \hat{\mathbf{z}})]. \quad (19)$$

In Figures 3 and 4 the abscissa $\alpha = \Delta\lambda/E_0$ is scaled with the Holtsmark field

$$E_0 = \frac{2.603 Z_P^{1/3} e N_e^{2/3}}{4\pi\epsilon_0}$$

where N_p denotes the perturbed density $N_p = N_e/Z_p$.

The same line of reasoning applies to the well-known hydrogenic lines $2P$–$4Q(Q = P,D,F)$ located at 4471 and 4921 Å in the spectrum of neutral helium (Deutsch, 1970).

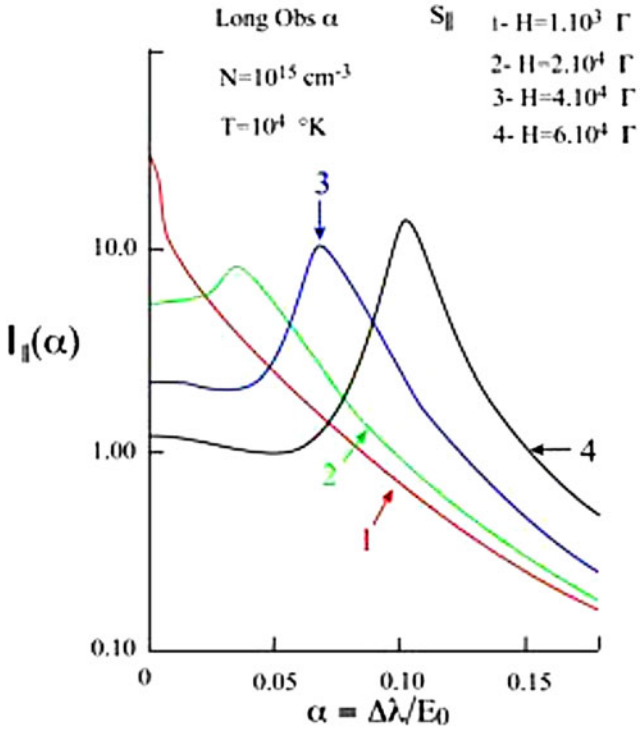

Fig. 3. Calculated H_α profile observed longitudinally $N_e = 10^{15}$ cm^{-3}; $T = 10^4$K, $H = 10^3\Gamma$ ($\tau = 15.44$) (1), $H = 2\times10^4\Gamma$ ($\tau = 0.7715$) (2), $H = 4\times10^4\Gamma$ ($\tau = 0.3857$) (3), $H = 6\times10^4\Gamma$ ($\tau = 0.2638$) (4) [after Nguyen-Hoe *et al.* (1967)].

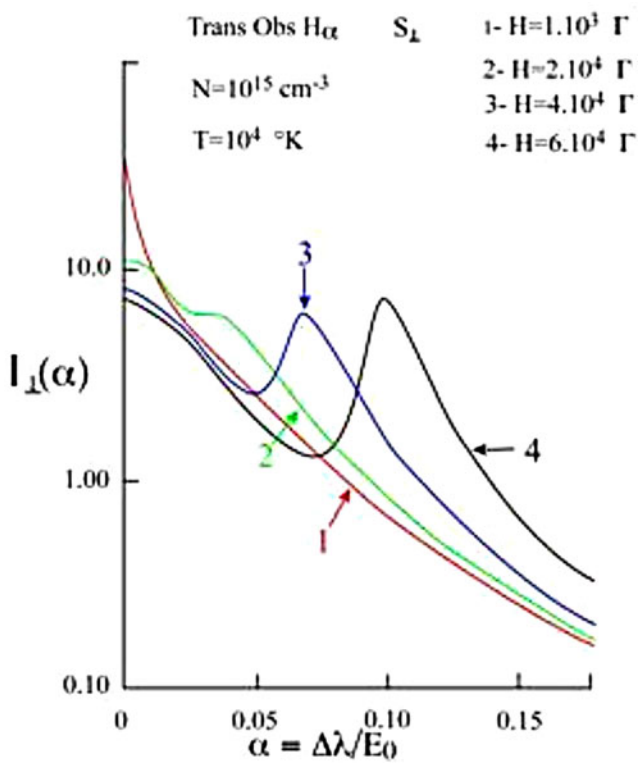

Fig. 4. Calculated H_α profile observed transversally $N_e = 10^{15}$ cm^{-3}; $T = 10^4$ K, $H = 1\times10^3\Gamma$ ($\tau = 15.44$) (1), $H = 2\times10^4\Gamma$ ($\tau = 0.7715$) (2), $H = 4\times10^4\Gamma$ ($\tau = 0.3857$) (3), $H = 6\times10^4\Gamma$ ($\tau = 0.2638$) (4) [after Nguyen-Hoe *et al.* (1967)].

Corresponding polarized profiles are exhibited on Figure 5.

At first sight, the given profiles show a structure which looks very different from the isolated-line Lorentz triplet and from the hydrogen H_β line broadened in the presence of a strong magnetic field with the same (N_e,T_e) values.

More precisely, the parallel intensities $I_{\parallel}(\Delta\lambda)$ keep their central peaks $2P$–$4D$ and $2P$–$4F$. The perpendicular intensities $I_{\perp}(\Delta\lambda)$ again exhibit this structure, but with a strong asymmetry. The second peak of $I_{\parallel}(\Delta\lambda)$ may be surely attributed to the $2P$–$4F$ maximum, as would be shown in a plot of $I(\Delta\lambda, \hat{\mathbf{z}})$ (polarized along the magnetic field and free from the σ components) with the same two-peaked structure.

Another striking result is the absence of σ components on the $2P$–$4D$ side and the appearance of a weak σ component on the $2^3P - 4^3F$ side only, located at

$$\Delta\lambda_z = \lambda^2 \times 4.688 \times 10^{-13} B, \quad \tau = 0.9 \quad (20)$$

where λ_z and λ are in angstroms, and B in gauss (see Fig. 6). This feature is easily explained by the interpenetration of the $2P$–$4D$ and $2P$–$4F$ static patterns in the presence of a strong Zeeman effect and also by the dominating electron-impact effect in the line center, at the vicinity of the $2P$–$4D$ maximum. This behavior is more pronounced for the 4^1Q sublevels, which have a stronger mutual interaction, than for the

https://doi.org/10.1017/S0263034615000919 Published online by Cambridge University Press

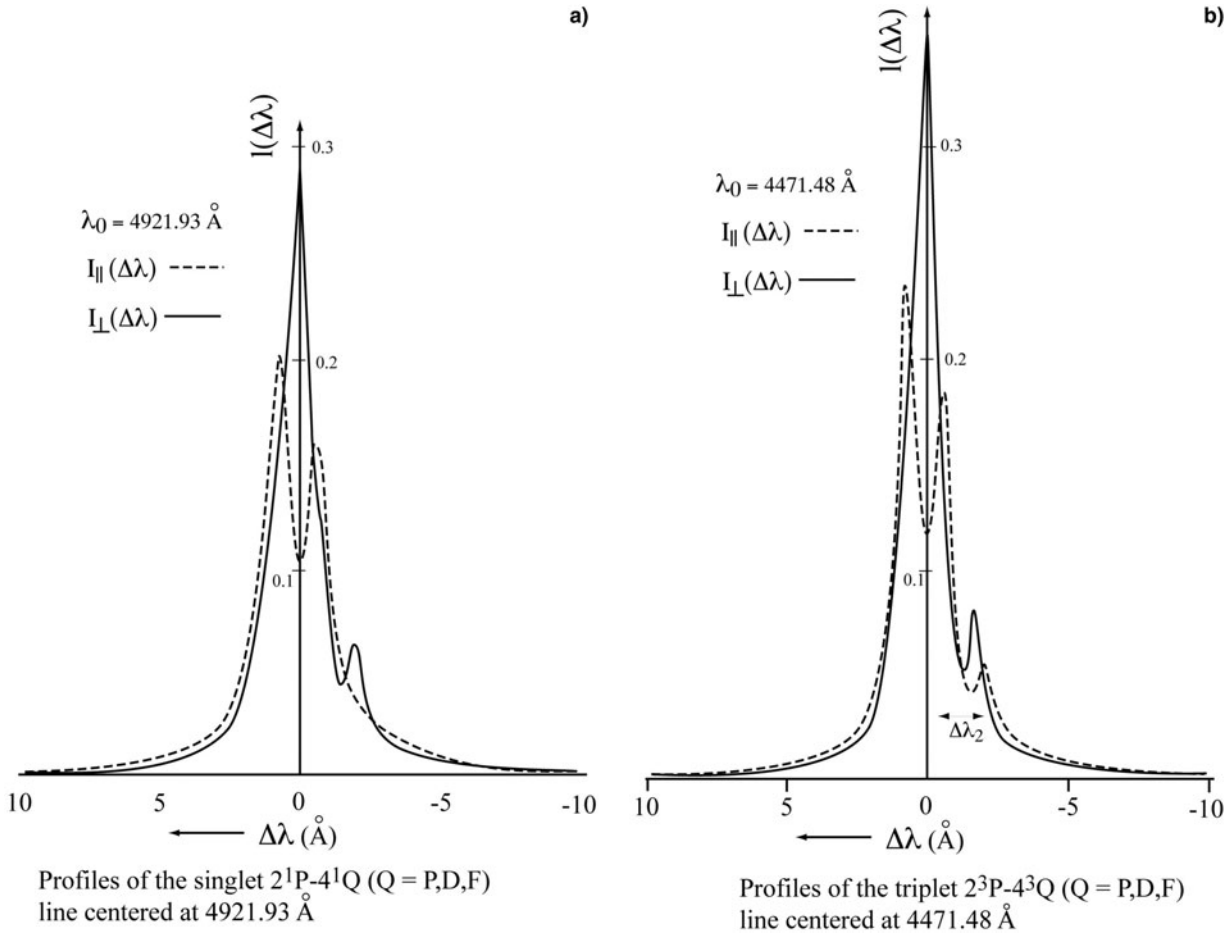

Fig. 5. Balmer-like transitions in neutral Helium. $N_e = 6 \times 10^{15} \mathrm{cm}^{-3}$, $T_e = 2 \times 10^4$ K, $H(G) = 7 \times 10^4$ [after Deutsch (1970)].

4^3Q ones. In fact, the line-center broadening of these partially degenerate lines is the result of a competition between Zeeman, static Stark, and electron-impact broadening.

As a by-product it clearly appears that even a strong Zeeman effect cannot be studied with a linear superposition of Lorentz triplets to each component of the static Stark pattern.

These considerations have been very recently extended to high-Z emitters (Iglesias, 2013) submitted to a combined Stark–Zeeman broadening mechanism, through a global algorithm presentation.

6. ION STOPPING IN MAGNETIZED PLASMA: A DIELECTRIC APPROACH

For many years, a high level of sophisticated and theory activity has been devoted to the stopping of nonrelativistic charged particles in arbitrary magnetized plasmas (see for instance Nersisyan *et al.*, 2007). However, the experimental vindication of this work is still badly missing. In order to promote a basic science approach easing quantitative studies of ion-magnetized plasma target, we intend to pinpoint – a few conspicuous trends suggested by theory or simulation studies.

6.1. Projectile velocity $V \geq V_{\mathrm{the}}$

At $V \geq V_{\mathrm{the}}$, target thermal electron velocity, one expects target ions to remain as a negligible contribution to the ion projectile showing down.

A first look at $\vec{V} \| \vec{B}$, steady applied magnetic field, one observes (see Fig. 6) a marked shift at $u = V/V_{\mathrm{the}} > 1$ of the maximum projectile stopping, toward the right of its usual location at $u \sim 1$ for $B = 0$.

Usually, one uses a finite series representation (Cereceda *et al.*, 2000), with a large number of terms (here $L = 250$ in the stopping expression (Ichimaru, 1973)

$$\frac{dE}{dt} = \frac{q^2}{2\pi^2 \epsilon_0} \int_0^{k_{\perp \max}} dk_\perp \cdot \int_0^\infty dk_\parallel \sum_{\ell=-\mathrm{L}}^{\mathrm{L}} k_\perp J_l^2(k_\perp \rho_{\mathrm{L}}) \times \frac{k_\perp v_\perp + \ell \omega_{\mathrm{c}}}{k^2} I_{\mathrm{m}} \left(\frac{-1}{\epsilon(\mathbf{k}, k_\perp v_\perp + \ell \omega_{\mathrm{c}})} \right). \tag{21}$$

where q is the projectile charge, ω_{c} its cyclotron frequency and $\rho_{\mathrm{L}} = V_\perp / \omega_{\mathrm{c}}$, its Larmor radius, in terms of the usual longitudinal dielectric function.

Another striking trend is the slowing down θ-dependence, where θ denotes the angle between $\vec{V}$ and $\vec{B}$. It features a monotone decay with increasing θ (see Fig. 7).

https://doi.org/10.1017/S0263034615000919 Published online by Cambridge University Press

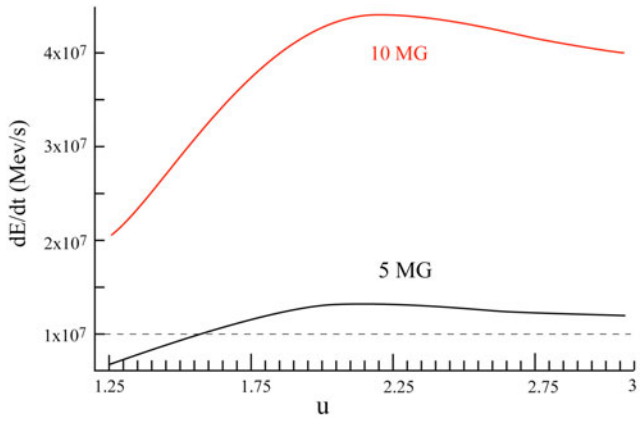

Fig. 6. Energy loss of α particles moving parallel to B as a function of dimensionless speed u, $N_e = 10^{21}\,\mathrm{cm}^{-3}$, $T = 5$ keV, $B = 5$ and 10 MG, [after Cereceda *et al.* (2000)].

6.2. $V < V_{\mathrm{the}}$

The low ion velocity slowing down (LIVSD) regime is also endowed with specific behaviors. When a simple kinetic-theoretic approach is applied to this regime, one easily faces basic conceptual difficulties (Nersisyan *et al.*, 2007) for $\theta = 0$ and $\pi/2$. A first and preliminary step out of this dilemma is to work within a hydrodynamic framework. We thus implement a radically novel approach to LIVSD when the projectile velocity v remains smaller than the target electron thermal v_{the}. We, thus consider ion stopping

$$S(V) \equiv \frac{dE_b}{dx}(V), \tag{22}$$

near $v = 0$. The ratio $S(V)/V$ usually monitors a linear stopping profile, up to 100 keV/a.m.u in cold matter. Similar trends are also reported in highly ionized plasma with $B = 0$ or $B \neq 0$.

From now on, we intend to make use of a very powerful connection between very low velocity ion stopping and particle diffusion through Einstein characterization of ion mobility associated with thermal electron fluctuations in target, around the slow ion projectile visualized as an impurity immersed in a dense and homogeneous electron fluid.

Technically, we are then led to use the recently proposed and exact Dufty–Berkovsky relationship

$$\lim_{v\to 0} \frac{S(V)}{V} = k_B T_e D^{-1}, \tag{23}$$

connecting the ratio of stopping to v in the zero velocity limit with the ion diffusion coefficient D in the target.

In a magnetized plasma D can be readily expressed in terms of Green–Kubo integrands (GKI) involving field fluctuations in the target electron fluid, under the form

$$D = \frac{c^2}{B^2}\int_0^\infty d\tau \langle \mathbf{E}(\tau)\cdot\mathbf{E}(0)\rangle \tag{24}$$

in terms of an equilibrium canonical average of the two-point autocorrelation function for fluctuating electric fields.

At this juncture we need to frame the GKI in suitable magnetized one-component plasma (OCP) models for the transverse and parallel geometry, respectively. This procedure implies that the slowly incoming ions are evolving against a background of faster fluctuating target electrons ($v < V_{\mathrm{the}}$) providing the OCP rigid neutralizing background thus validating the OCP assumption.

Moreover, restricting to proton projectiles impacting the electron–proton plasma we immediately perceive the pertinence of the diffusion-based LIVSD as phrased by Eq. (23).

First, the proton beam can easily self-diffuse amongst its target homologues, while the same mechanism experienced by target electrons allow them to drag ambipolarly the incoming proton projectiles.

So, the transverse electron LIVSD can either be monitored by the well-known classical diffusion $D_\perp \sim B^{-2}$, or by the Bohm-like hydrodynamic one with $D_\perp \sim B^{-1}$. In the first case, momentum conservation at the level of the electron–ion pair implies that the ions will diffuse with the same coefficient as the electrons. On the other hand, the hydro Bohm diffusion across **B** is operated through clumps with a large number of particles involved in this collective process.

So, exploring first the $\omega_b \geq \omega_p$ domain, one can explicit the parallel and B-independent diffusion

$$D_\parallel^{(0)} = \frac{2\sqrt{\pi}V_{\mathrm{thi}}^2}{\nu_c} \sim \mathrm{O}(\omega_b^0), \tag{25}$$

yielding back readily the unmagnetized ($B = 0$) LIVSD where $V_{\mathrm{thi}}^2 = k_B T/M_i$, and $\nu_c = \omega_p \varepsilon_p ln(1/\varepsilon_p)$ in terms of the redefined dimensionless plasma parameter $\varepsilon_p = 1/n_e\lambda_D^3$, and λ_D, the Debye length, in a beam-plasma system taken as globally neutral with $\nu_c/\omega_b \ll 1$.

At the same level of approximation transverse diffusion reads as

$$D_\perp^{(0)} = \frac{r_L^2 \nu_c}{3\sqrt{\pi}} \sim \mathrm{O}(\omega_b^{-2})$$

in terms of Larmor radius $r_L = V_{\mathrm{thi}}/\omega_b$.

With higher B values ($\omega_b \gg \omega_p$) one reaches the transverse hydro Bohm regime featuring (Marchetti *et al.*, 1984)

$$D_\perp = D_\perp^0 + \frac{0.5 V_{\mathrm{thi}}^2}{\omega_b}\epsilon_p^2[\ln(1/\varepsilon_p)]^{3/2}, \tag{26}$$

while parallel diffusion retains a ω_b-dependence through

$$D_\parallel^{(0)} = \frac{\Gamma^{5/2}}{\omega_p a^2}\left(\frac{3}{\pi}\right)^{1/2}\left[0.5\ \ln(1+X^2) - 0.3 + \frac{0.0235}{r^2}\right], \tag{27}$$

where $\Gamma = a^2/3\lambda_D^2$ with $a = (3/4\pi n_e)^{1/3}$, $r = \omega_p/\omega_b$ and $X = 1/\sqrt{3}\Gamma^{3/2} < 1$ encompasses, most if not all, situations of practical interest.

https://doi.org/10.1017/S0263034615000919 Published online by Cambridge University Press

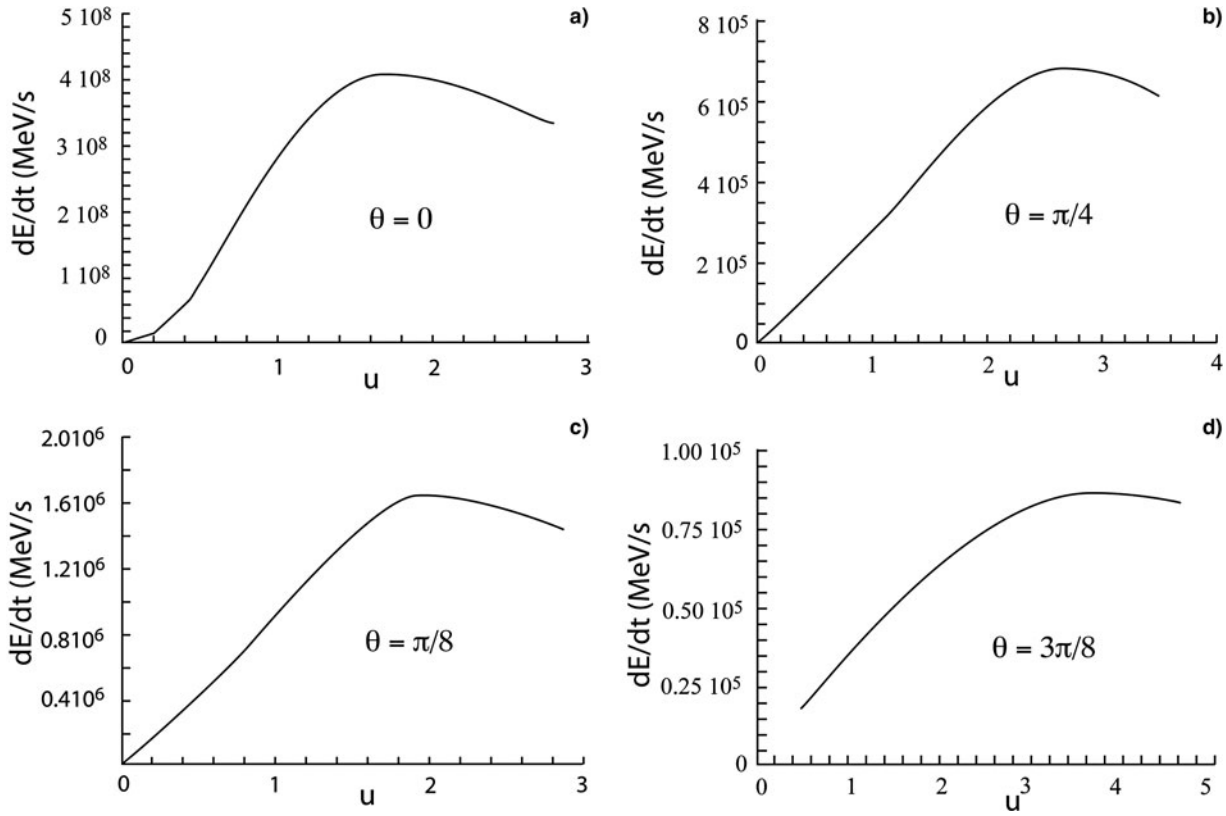

Fig. 7. Energy loss of α particles moving at angle θ with respect to B as a function of dimensionless speed $u = V/V_{\text{the}}$. (**a**) $\theta = 0$, (**b**) $\theta = \pi$, (**c**) $\theta = \pi/4$, (**d**) $\theta = 3\pi/8$. $N_e = 10^{21}$ cm^{-3}, $T_e = 5$ keV, $B = 500$ T [after Cereceda *et al.* (2005)].

When electron diffusion is considered, v_{the} should be used in Eq. (26) and the above ambipolar process has to be implemented.

The $D_\perp$ and $D_\parallel$ expressions introduced in Eqs (26) and (27) are expected to document a strong anisotropy between transverse and parallel slowing down. However, in both cases, B-dependence is obviously increasing with B^2 (classical) or B (Bohm-like). The temperature behavior is much more intriguing, as respectively displayed on Figures 8 and 9 for transverse and parallel LIVSD. One, then witnesses a monotonous increase for transverse stopping (Fig. 8) contrasted to a monotonous decay for parallel counterpart (Fig. 9).

We thus implemented the very simple LIVSD expression (23) to the, *a priory* very involved ion beam-arbitrarily magnetized plasma interaction. We used transverse and parallel diffusion coefficients in suitably framed magnetized OCP with target electrons building up the corresponding

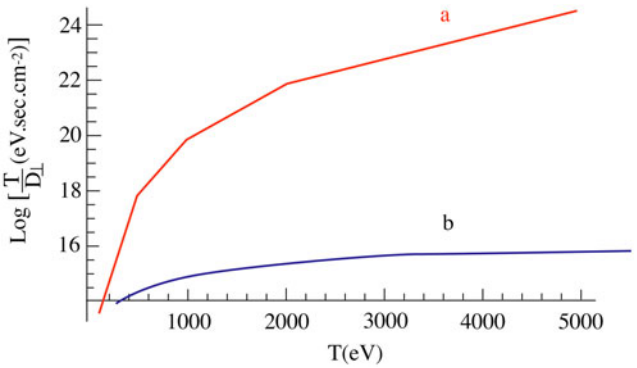

Fig. 8. Proton transverse LIVSD in a dense plasma ($n = 10^{21}$ cm^{-3} and $B = 10^{10}$ G). (**a**) Electron stopping, (**b**) ion stopping, [after Deutsch & Popoff (2008)].

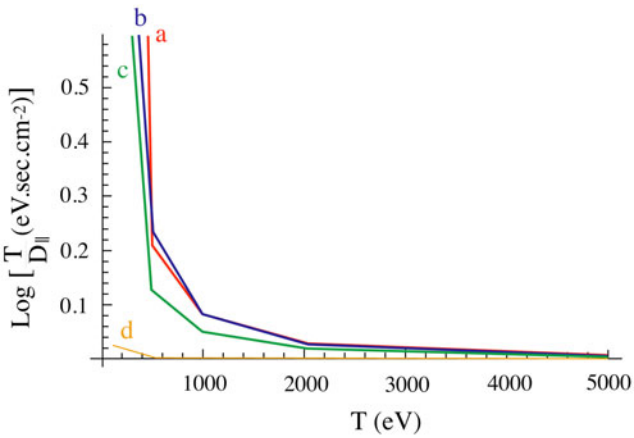

Fig. 9. Proton parallel LIVSD in a dense plasma ($n = 10^{21}$ cm^{-3} and $B = 10^{10}$ G). (**a**) Electron stopping ($B \neq 0$), (**b**) ion stopping ($B \neq 0$), (**c**) ion stopping ($B = 0$), (**d**) electron stopping ($B = 0$) [after Deutsch & Popoff (2008)].

https://doi.org/10.1017/S0263034615000919 Published online by Cambridge University Press

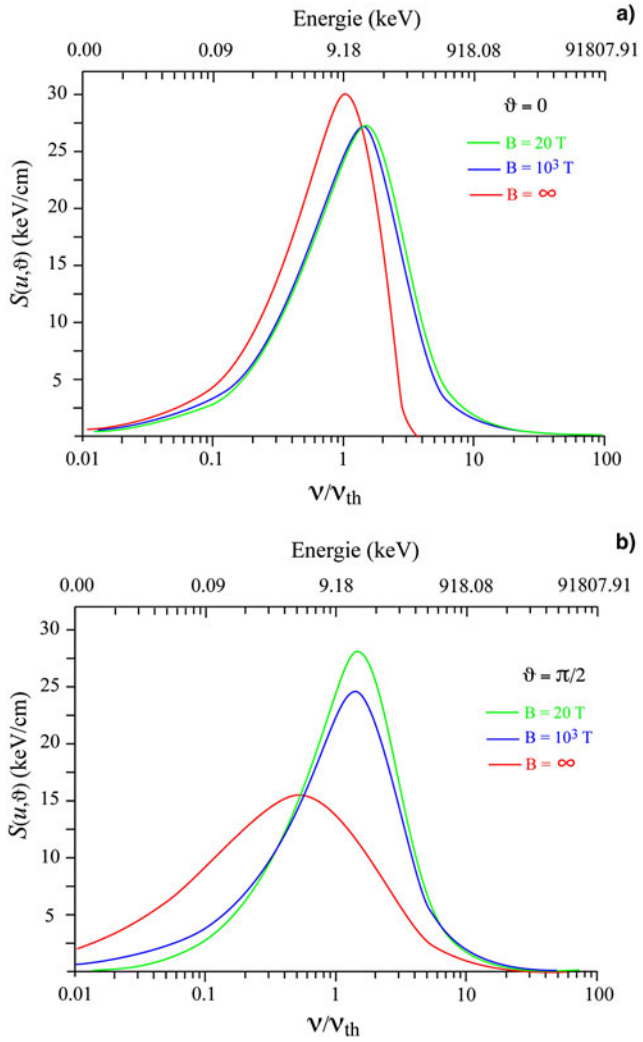

Fig. 10. Proton stopping in a magnetized electron–proton plasma ($n_e = 10^{18}$ cm^{-3}; $T = 10$ eV). (**a**) $\theta = 0$, (**b**) $\theta = \pi/2$.

neutralizing background. Thus, we reached analytic LIVSD transverse and parallel expressions.

Finally, we investigate the stopping power of an ion in a magnetized electron plasma in a model of binary collisions (BC) between ions and magnetized electrons, in which the Coulomb interaction is treated up to second-order as a perturbation to the helical motion of the electrons. The calculations are done with the help of an improved BC theory which is uniformly valid for any strength of the magnetic field and where the second-order two-body forces are treated in the interaction in Fourier space without specifying the interaction potential. The stopping power is explicitly calculated for a regularized and screened potential which is both of finite range and less singular than the Coulomb interaction at the origin. Closed expressions are derived for mono-energetic electrons, which are then folded with the velocity distributions of the electrons. The resulting stopping power is evaluated for isotropic Maxwell velocity distributions of the electrons. The accuracy and validity of the present model have been studied by comparisons with the classical trajectory Monte Carlo numerical simulations.

Finally, with a view toward possible experiments envisioned at LULI (Palaiseau) or TITAN (Livermore) with PW-laser produced protons, we propose to check at $B = 20$ T, the $\theta = 0$ and $\pi/2$ data obtained with the present kinetic-elaborated formalism (Fig. 10).

7. SUMMARIES

Out of the above surveyed diagnostics for dense and magnetized plasmas of ICF interest, we stress emphasis on the following suggestions:

- The IFE needs a basic theory simulation revisitation in order to match quantitatively present day available experimental vindication.
- TS in a magnetized plasma is presently restricted to dilute and Tokamak-like situations. It has to be extended to dense and hot plasmas envisioned for ICF.
- Combined Stark–Zeeman line broadening requires to be adapted to high-Z elements (Iglesias, 2013) and eventually compared with fine and hyperfine line splitting. Moreover the spiraling of perturbing charges around the emitter has to be tackled for Larmor radii smaller than Debye lengths.

As far as we know, the above panorama of potentially available diagnostics for strongly magnetized ICF-like plasmas is here critically displayed for the first time. Such a presentation is primarily motivated by novel experimental achievements (Fujioka *et al.*, 2013) allowing for a very efficient and nearly steady magnetization process, far beyond those previously proposed for magnetized target fusion (for instance Cereceda *et al.*, 2000).

We hope that the above speculations could be appreciated as timely ones in view of the increasing interest within the inertial fusion community for the investigation of ultra-dense plasmas exposed to kilo Teslas steady magnetic fields. In particular, it is highly likely that an imposed magnetization on inertial pellet could allow for a better control of its compression in a large setup of the NIF–LeMegaJoule (LMJ) class.

REFERENCES

Bekefi, G., Deutsch, C. & Ya' akobi, B. (1976). Spectroscopic diagnostics of laser plasmas. In *Principles of Laser Plasmas* (Bekefi, E.G. Ed.), pp. 549–569. New York: Wiley Interscience.

Cereceda, C., Deperetti, M. & Deutsch, C. (2005). Stopping power for arbitrary angle between test particle velocity and magnetic field. *Phys. Plasma* **12**, 022102.

https://doi.org/10.1017/S0263034615000919 Published online by Cambridge University Press

Cereceda, C., Deutsch, C., Deperetti, M., Sabatier, M. & Nersisyan, H.B. (2000). Dielectric response function and stopping power of dense magnetized plasma. *Phys. Plamas* **7**, 2884–2893.

Chou, C.K. & Chen, H.H. (1994). Stokes parameters for Thomson scattering in a cold magnetized plasma. *Astrophys. Space Sci*. **218**, 87–100.

Deschamps, J., Fitaire, M. & Lagoute, M. (1970). Inverse Faraday effect in a plasma. *Phys. Rev. Lett*. **25**, 1330–1333.

Deutsch, C. (1970). Influence of a strong magnetic field on plasma – broadened 2P – 4P, 2P – 4D and 2P – 4F He (I) lines. *Phys. Rev*. **A2**, 1258–1261.

Deutsch, C. & Popoff, R. (2008). Low ion – velocity slowing down in a strongly magnetized target plasma. *Phys. Rev*. **E78**, 056405–8.

Eliezer, S. (2002). *The Interaction of High – Power Lasers with Plasmas*. Bristol, Philadelphia: Institute of Physics.

Fujioka, S., Zhang, Z., Ishihara, K., Shigemori, K., Hironaka, Y., Shiraga, H., Nishimura, H. & Azechi, H. (2013). KiloTesla magnetic field due to a capacitor – coil target driven by high – power laser. *Sci. Rep*. **3**, 1170–1179.

Griem, H.R. (1964). *Plasma Spectroscopy*. New York: Mc Graw-Hill Co.

Horovitz, Y., Eliezer, S., Ludminski, A., Henis, Z., Moshe, E., Shpitalnik, R. & Arad, B. (1997). Measurements of inverse Faraday effect absorption of circularly polarized laser light in plasmas. *Phys. Rev. Lett*. **78**, 1797–1800.

Ichimaru, S. (1973). *Basic Principles of Plasma Physics: A Statistical Approach*. Reading, MA: W.A. Benjamin.

Iglesias, C. (2013). Efficient algorithms for Stark – Zeeman spectral line shape calculations. *High Energy Density Phys*. **9**, 737–744.

Kenmochi, N., Minami, C., Takahashi, S., Mizuuchi, T., Kobayashi, S., Nagasaki, K., Nakamura, Y., Okada, S., Yamamoto, S., Oshima, S., Konoshima, S., Shi, N., Zang, L., Kasajima, K. & Sano, F. (2014). First measurements of time evolution of electron temperature profiles with Nd:YAG Thomson scattering system on Heliotron. *J. Rev. Sci. Instrum*. **85**, 11D819-3.

Lehner, T. (1994). Intense magnetic – field generation by relativistic ponderomotive force in an underdense plasma. *Phys. Scr*. **49**, 704–711.

Marchetti, M.C., Kirkpatrick, T.R. & Dorfman, J.R. (1984). Anomalous diffusion of charged particles in a strong magnetic field. *Phys. Rev. A* **29**, 2960–2962.

Najmudin, Z., Tatarakis, M., Pukhov, A., Clark, E.L., Clarke, R.J., Dangor, A.E., Faure, J., Malka, V., Neely, D., Santala, M.I.K. & Krushelnik, K. (2001). Measurements of the inverse Faraday effect from relativistic interactions with an underdense plasma. *Phys. Rev. Lett*. **87**, 21500–21503.

Nersisyan, H.B., Toepffer, C. & Zwicknagel, G. (2007). *Interactions between Charged Particles in a Magnetic Field*. Berlin – Heidelberg: Springer – Verlag.

Nguyen – Hoe, Drawin, H.W. & Herman, L. (1967). Effet d'un champ magnétique uniforme sur les profils des raies de l'hydrogène. *J. Quant. Spectrosc. Radiat. Transf*. **7**, 429–474.

Potekhin, A.Y. & Chabrier, G. (2012). Equation of state for magnetized Coulomb plasmas. *Astron. Astrophys*. **550**, A43.

Sheffield, J. (1975). *Plasma Scattering of Electromagnetic Radiation*. New York: Academic Press.

Talin, B. Kaftandjian, V.P. & Klein, L.S. (1975). Inverse Faraday effect in plasmas. *Phys. Rev. A* **11**, 648–665.

https://doi.org/10.1017/S0263034615000919 Published online by Cambridge University Press